https://doi.org/10.5194/cp-2021-30
Preprint. Discussion started: 3 May 2021

Climate of the Past Discussions

CHELSA-TraCE21k v1.0. Downscaled transient temperature and precipitation data since the last glacial maximum

Dirk Nikolaus Karger[1], Michael P. Nobis[1], Signe Normand[2], Catherine H. Graham[1], Niklaus E. Zimmermann[1]

[1]Swiss Federal Research Institute WSL, Zürcherstrasse 111, 8903 Birmensdorf, Switzerland
[2]Aarhus University, Ny Munkegade 116, 8000 Aarhus, Denmark

Correspondence to: Dirk N. Karger (dirk.karger@wsl.ch)

Abstract. High resolution, downscaled climate model data are used in a wide variety of applications across environmental sciences. Here we introduce the CHELSA-TraCE21k downscaling algorithm to create global monthly climatologies for temperature and precipitation at 30 arcsec spatial resolution in 100-year time steps for the last 21,000 years. Paleo orography at high spatial resolution and at each timestep is created by combining high resolution information on glacial cover from current and Last Glacial Maximum (LGM) glacier databases with the interpolation of a dynamic ice sheet model (ICE6G) and a coupling to mean annual temperatures from CCSM3-TraCE21k. Based on the reconstructed paleo orography, mean annual temperature and precipitation was downscaled using the CHELSA V1.2 algorithm. The data were validated by comparisons with the glacial extent of the Laurentide ice shield based on expert delineations, proxy data from Greenland ice cores, historical climate data from meteorological stations, and a dynamic simulation of species distribution throughout the Holocene. Validations show that CHELSA TraCE21k output creates a reasonable representation of the distribution of temperature and precipitation through time at a high spatial resolution, and simulations based on the data are capable of detecting effective LGM refugia of species.

1 Introduction

Since the Last Glacial Maximum (LGM), variation in climate has caused multiple changes of the Earth surface, including the rearrangement of species distributions, or even extinctions (Adams and Faure, 1997; Binney et al., 2017; Prentice et al., 1991; Velichko et al., 1997; Williams et al., 2004; Yu et al., 2010). Yet we have not fully evaluated the historical underpinnings of these changes as we have often lacked the climate data at the necessary spatial resolution. Biological entities such as species usually encounter climatic conditions at spatial resolutions (<1km^2) (Seo et al., 2009) that are not captured by numerical global circulation models (GCMs) which run at much coarser grains (e.g. >0.5°). For many applications such as inference of ecological niches (Hutchinson, 1957), determination of growing seasons (McMaster and Wilhelm, 1997), identification of species migrations (Engler and Guisan, 2009), or modelling of high resolution species distributions (Guisan and Thuiller, 2005; Guisan and Zimmermann, 2000), temporal and spatial variability in temperature and precipitation is highly important. For such analyses, errors in the underlying climate data can strongly deteriorate the analytical power (Soria-Auza et al., 2010).

https://doi.org/10.5194/cp-2021-30
Preprint. Discussion started: 3 May 2021


Climate of the Past Discussions

For the recent past the gap between the coarse GCM resolution and the high resolution needed has be bridged using satellite data (Biasutti et al., 2011; Funk et al., 2015; Huffman et al., 2007), statistical downscaling (Karger et al., 2017a, 2020; Maraun et al., 2010; Schmidli et al., 2006; Wilby et al., 1998; Wood et al., 2004), dynamical downscaling (Skamarock et al., 2019), or interpolation of meteorological station data (Daly et al., 1997; Harris et al., 2020; Hijmans et al., 2005; Meyer-Christoffer et al., 2015). While all of these methods work comparably well for current climatic conditions, satellite or station data are not available before the 19th Century (end of the 20th century for satellite data), hampering an application of said methods to paleo-climatic models. Most paleoclimatic data at high spatial resolution is therefore based on climatologically aided interpolation of GCM output (Brown et al., 2018). This process uses the high-resolution information of current day climatologies, and adds an interpolated anomaly derived from a coarser-resolution GCM (Hunter and Meentemeyer, 2005; Willmott and Robeson, 1995). While this approach works rather well for short term time series where topography is relatively stable (Daly et al., 1997), it becomes difficult for longer time series where the dependence structure between variables (e.g. topography and climate) is dynamic (Maraun, 2013). This phenomenon is of concern especially in the last 21'000 years, as the topography in many regions on earth has changed drastically due to the retreating ice shields and glaciers along the poles and in high mountain areas (Scotese, 2001). While numerical climate models are able to simulate paleo-environmental conditions comparably well (Sepulchre et al., 2020), they are however, computationally very demanding, and therefore they have not been applied on ecologically relevant spatial resolutions of ~1km yet. Current global kilometer-scale models only show a simulation throughput of 0.043 SYPD (simulated years per day) (Fuhrer et al., 2018), which is 25-fold lower than computater-efficient simulations of 1 SYPD (Schär et al., 2019; Schulthess et al., 2018). Even with state-of-the-art supercomputers and climate models this gap can only be minimized by a factor of 20 (Neumann et al., 2019).

Climate impact studies however, often only use a reduced set of climate variables compared to those available from the numerical output of climate models (Frieler et al., 2017). Such studies do not need therefore a complete representation of all climate processes at high spatial resolution. In ecological studies, for instance, precipitation is often used along with minimum and maximum temperatures for analyses of species occurrences (Woodward et al., 1990). Also, it is common practice to describe species ranges by their climate envelopes and building species distribution models (SDMs) with a relatively small set of climate predictors based on monthly minimum and maximum temperature and precipitation (Guisan and Thuiller, 2005; Guisan and Zimmermann, 2000).

Here we present paleo-climatic data, downscaled from the CCSM3_TraCE21k model to a 30 arcsec resolution using the CHELSA V1.2 algorithm (Karger et al., 2017a), which covers time steps of 100 years from 21k-BP to 1990, for minimum and maximum temperatures, surface precipitation, and paleo-orography.

https://doi.org/10.5194/cp-2021-30
Preprint. Discussion started: 3 May 2021


Climate of the Past Discussions

2 Input data

2.1 Transient climate simulations: CCSM3 TraCE-21k

The CCSM3 TraCE-21k climate model (Carlson et al., 2012; He, 2011; Liu et al., 2009; Marcott et al., 2011) provides information on climate change over the last 21,000 years, i.e. from Last Glacial Maximum (LGM) to present. The TraCE-21k simulations are capable to reproduce many main features of post-glacial climate dynamics in various parts of the world form low to high latitudes and including abrupt climate changes (He, 2011; Liu et al., 2009). CCSM3 TraCE-21k uses the Community Climate System Model version 3 (CCSM3)of the National Center for Atmospheric Research (NCAR), which is a global climate model with coupled ocean, atmosphere, sea ice, and land surface components (Collins et al., 2006). CCSM3 TraCE-21k was calculated at T31_gx3v5 resolution (Otto-Bliesner et al., 2006) using a coarse resolution dynamic global vegetation model (DGVM) together with the Community Atmospheric Model 3 (CAM3), on 26 vertical hybrid coordinate levels. The land and atmosphere model use the same resolution. The parameterizations of dynamic vegetation model is largely based on the Lund-Potsdam-Jena (LPJ)-DGVM. The ocean model in CCSM3-TraCE21k uses the NCAR version of the Parallel Ocean Program (POP) with 25 vertical levels and the sea ice model is the NCAR Community Sea Ice Model (CSIM).

2.2 Observational climatology: CHELSA V1.2

CHELSA is a high-resolution (30 arcsec) climate data set for earth land surface areas (Karger et al., 2017b, 2017a). It includes monthly mean temperature and precipitation grids for the time period 1979-2013. CHELSA uses a quasi-mechanistical statistical downscaling of the ERA interim reanalysis (Berrisford et al., 2009) with a GPCC (Meyer-Christoffer et al., 2015) bias correction.

2.2 Transient glacial extent simulations: ICE6G_C

The ICE6G_C model is a refinement of the ICE5G (VM2) model (Peltier, 2004) which has been widely used to model the distribution and dynamics of major ice shields through time. The ICE6G_C explicitly models changes in ice thickness of major ice sheets (e.g. the Laurentide ice sheet) from Last Glacial Maximum (LGM) till today (Argus et al., 2014; Peltier et al., 2015) at 500 year time steps.

2.3 Observational glacial extent at Last Glacial Maximum (LGM)

As the extent of the glaciers during LGM, we use data from Ehlers et al. (2011) that presents an up-to-date, detailed overview of Quaternary glaciations all over the world, not only with regard to stratigraphy but also with regard to major glacial landforms and the extent of the respective ice sheets.

https://doi.org/10.5194/cp-2021-30
Preprint. Discussion started: 3 May 2021


Climate of the Past Discussions

2.4 Observational current glacial extent: GLIMS

The GLIMS (Global Land Ice Measurements from Space) project (Raup et al., 2007) at the NSIDC (National Snow and Ice Data Center) provides data on global glacial extent and other information about glaciers including metadata on how those outlines were derived. Here we use this database to delineate the current extent of the glaciers at high resolution globally.

3 Methods:

Downscaling is based on a derived version of the CHELSA V1.2 algorithm (Karger et al., 2017a) and forcings from CCSM3 TraCE-21k (He, 2011; Liu et al., 2009) and involved four main steps. (1) To apply the CHELSA algorithm on the TraCE-21k data, we first approximated the paleo-orography using a combination of data from the digital elevation model GMTED2010 (Danielson and Gesch, 2011), large scale ice sheet configurations from ICE6G (Peltier et al., 2015), high resolution glacier extents from GLIMS (Raup et al., 2007) and (Ehlers et al., 2011), as well as sea level change data from (Miller et al., 2005). Subsequently, we coupled the paleo-orography with (2) temperature and (3) precipitation, and (4) validated the resulting climatology.

3.1 Paleo-orography

The first step in the downscaling was to combine annual mean temperature data with sea surface elevation and ICE6G data to estimate combined ice + surface orography. The rationale behind this approach is that temperature and glacier extents are to some degree interdependent, and a change in temperature will translate to a change in glacial extent. This approach was implemented by first combining the high resolution glacial extents from (Ehlers et al., 2011) with the ICE6G data. To do so, we randomly sampled 100 point location per 1° grid cell from ICE6G and extracted the height of the glacier plus the surface elevation e_t^{ice} at time 0 (LGM). All points that did not fall within the high-resolution glacial extent were omitted. We then converted the polygons of the glacial extents into point locations as well, and extracted their elevation e_{G_t} from the DEM at time e_t^{dem}, where $e_t^{dem} = e^{dem} - e_s$ with e_s being the difference between the current and past sea surface elevation at time *t*. Then both point datasets were combined to e_t^{obs} containing a point sample of the surface orography. This point sample was then spatially interpolated to a grid of 30 arcsec resolution applying multilevel B-spline interpolation. The multilevel B-splines use a B-spline approximation to e_t and starts using the coarsest grid ϕ_0 from an overall set of grids $\phi_0, \phi_1, \ldots, \phi_n$ with $n = 14$ generated using optimized B-spline refinements (Lee et al., 1997). The resulting B-spline function $f_0(e_t^{obs})$ then gives the first approximation of e_t. $f_0(e_t)$ and leaves a deviation:

$$\Delta^1 {e_t^{obs}}_c = e_t^{obs} - f_0(x_c, y_c) \quad (1)$$

https://doi.org/10.5194/cp-2021-30
Preprint. Discussion started: 3 May 2021


Climate of the Past Discussions

at each location $(x_c, y_c, e_t^{obs}{}_c)$. Then the next control lattice ϕ_1 is used to approximate $f_1(\Delta^1 e_t^{obs}{}_c)$. This approximation is then repeated on the sum of:

$$f_0 + f_1 = e_t^{obs} - f_0(x_c, y_c) - f_1(x_c, y_c) \quad (2)$$

at each point $(x_c, y_c, e_t^{obs}{}_c)$ n times resulting, in our case, in the gap free interpolated glacial surface e_t^{int}. The interpolated glacial surface was then combined with e_{DEM_t} to the orography e_t^{oro} using:

$$e_t^{oro} = \{ e_t^{dem},\ e_t^{dem} \geq e_t^{int}\ e_t^{int},\ otherwise \quad (3)$$

3.2 Temperature coupling

The estimated orography at the LGM e_t^{oro} was then used to downscale mean annual temperature $tas_{t=0}$. GCMs such as the CCSM3 normally exhibit a large bias in temperatures or precipitation (Cannon et al., 2015; Maraun, 2013). We therefore applied a change factor bias correction on current mean annual temperatures tas_{cur}^{obs} from CHELSA V1.2 resampled to a 0.5° grid resolution, where the change factor was calculated from the $\Delta tas = tas_{cur}^{mod} - tas_t^{mod}$. This effectively preserves the trends observed in temperature, but simultaneously assumes that the bias has been conserved over time (Maraun, 2016). For the interpolation of Δtas to the 0.5° grid resolution of tas_{cur}^{obs} the same multilevel B-spline interpolation was used as described above. The bias corrected temperatures tas_t^{cor} are then given by $tas_t^{cor} = tas_{cur}^{obs} - \Delta tas$. To achieve a high-resolution temperature approximation, we used a lapse rate-based downscaling from atmospheric temperature data at the TraCE-21k pressure levels. The lapse rates Γ are based on a linear approximation from average temperatures ta_z at altitudes a_z at vertical levels 26 to 20 of the T31 grid so that:

$$\Gamma = \frac{n(\sum a_z ta_z) - (\sum a_z)(\sum ta_z)}{n(\sum a_z{}^2) - (\sum a_z)^2} \quad (4)$$

Temperature at the surface at a high spatial resolution tas was then calculated by:

$$tas_t = \Gamma_t * e_t^{oro} + tas_t^{cor} \quad (5)$$

To couple the outline of the glacier to the mean annual temperature, we transformed the glacier elevations $e_t^G = e_t^{dem} < e_t^{int}$, to a polygon, and then transformed the outline of this polygon to a point sampling of the glacier boundaries at time t: e_t^{GB}. Temperatures tas_t^{GB} at the glacier boundary where then extracted for each boundary location coordinate (x, y) during the

https://doi.org/10.5194/cp-2021-30
Preprint. Discussion started: 3 May 2021


Climate of the Past Discussions

LGM ($t = 0$) which gives the local temperature under which a glacial boundary existed during the LGM $\left(x_{tas_0^{GB}}, y_{tas_0^{GB}}\right)$. As this simple coupling between glacial boundaries and annual temperatures is however only a rough estimate, we additionally included current temperatures and calculated the difference between current and LGM boundary temperatures. Here, the locations for the current glacial boundaries were extracted $\left(x_{tas_{cur}^{GB}}, y_{tas_{cur}^{GB}}\right)$ and locations of current and LGM glacial boundary temperatures were combined. The resulting point locations were then interpolated using a multilevel-B-spline to result in a gap-free surface Δtas_{cur}^{obs}. As the orography for the next time step is not known yet, we estimated the near surface air temperature tas_{t+1}^{est} for the glacial melt similar the orography from the time step before. So that:

$$tas_{t+1}^{est} = \Gamma_{t+1} * e_t^{oro} + tas_{t+1}^{cor} \tag{6}$$

The binary glacial extent G_{t+1} at $t + 1$ is then approximated as:

$$G_{t+1} = \begin{cases} 1, \ tas_{t+1}^{est} < \ tas_t^{GB} + \frac{\Delta tas_{cur}^{obs}}{-1*(\sum t-t)} \wedge G_0 = 1 \\ 0, \ otherwise \end{cases} \tag{7}$$

here the second term in the condition for G_{t+1} linearly scales Δtas_{cur}^{obs} over the entire number of time steps. This correction is necessary, as otherwise the entire bias would be added at the first time step, resulting in an unrealistic strong shift in the glacial extent. We then repeated the transformation of the glacial extent G_{t+1} to all point locations and repeated the procedure for the temperature coupling to estimate the orography e_{t+1}^{oro}. Near surface air temperatures for $t + 1$ have been then approximated using:

$$tas_{t+1} = \Gamma_{t+1} * e_{t+1}^{oro} + tas_{t+1}^{cor} \tag{8}$$

3.3 Precipitation estimation

The estimation of high resolution precipitation follows a variant of the CHELSA V1.2 algorithm (Karger et al. 2017). The CHELSA V1.2 algorithm assumes elevation to be the main driver of vertical precipitation gradients, which is however, highly idiosyncratic (Basist et al., 1994; Böhner, 2006; Böhner and Antonic, 2009; Daly et al., 1997; Gao et al., 2006; Karger et al., 2017a; Sevruk, 1997; Spreen, 1947). In tropical convective regimes, precipitation typically increase up to the condensation level around 1000-1500 m above surface, while exponentially decreasing moisture content in the mid- to upper troposphere results in a drying above the condensation level resulting in non-linear precipitation lapse rates (Körner, 2007). Furthermore, negative precipitation lapse rates are common under the extremely dry polar climates. In contrast, at mid-latitudes and in the subtropics, precipitation generally increases with increasing elevation due to advection. As a consequence, summits of the

https://doi.org/10.5194/cp-2021-30
Preprint. Discussion started: 3 May 2021


Climate of the Past Discussions

Alps or other high mountain ranges exhibit high rainfall (Rotunno and Houze, 2007), and lapse rates for precipitation are almost linear (Weischet and Endlicher, 2008). To approximate the effects of orographic precipitation we used a variant of the CHELSA V1.2 algorithm, which is explained in detail below.

We used 10 m *u*-wind and *v*-wind of TraCE-21k to calculate wind direction. Both wind components were projected to a world Mercator projection and then interpolated to a 4 km grid resolution using a multilevel B-spline interpolation similar to the one used for the bias correction surface. Windward and leeward effects are assumed to be best represented at resolutions larger than 1km (Daly *et al.*, 1994), we therefore chose a grid resolution of 4km for the underlying digital elevation model. The wind effect H was then calculated using:

$$H_W = \frac{\sum_{i=1}^{n} \frac{1}{d_{WHi}} tan^{-1}\left(\frac{d_{WZi}}{d_{WHi}^{0.5}}\right)}{\sum_{i=1}^{n} \frac{1}{d_{LHi}}} + \frac{\sum_{i=1}^{n} \frac{1}{d_{LHi}} tan^{-1}\left(\frac{d_{LZi}}{d_{LHi}^{0.5}}\right)}{\sum_{i=1}^{n} \frac{1}{d_{LHi}}} \quad (9)$$

$$H_L \frac{\sum_{i=1}^{n} \frac{1}{\ln(d_{WHi})} tan^{-1}\left(\frac{d_{LZi}}{d_{WHi}^{0.5}}\right)}{\sum_{i=1}^{n} \frac{1}{\ln(d_{LHi})}} \quad (10)$$

where d_{WHi} and d_{LHi} refer to the horizontal distances between the focal 3km grid cell in windward and leeward direction and d_{WZi} and d_{LZi} are the corresponding vertical distances compared with the focal 3km cell following the wind trajectory. The second summand in the equation for H_W where $d_{LHi} < 0$ accounts for the leeward impact of previously traversed mountain chains. The horizontal distances in the equation for H_L where $d_{LHi} \geq 0$ lead to a longer-distance impact of leeward rain shadow. The final wind-effect parameter is calculated as $H = H_L H_W$. Both equations were applied to each grid cell at the 30 arc sec. resolution in a World Mercator projection. Orographic precipitation effects are less pronounced just above the surface, as well as in the free atmosphere above the planetary boundary layer (Daly et al., 1997; Karger et al., 2020; Oke, 2002; Stull, 2012). The highest impact of orography is considered just at the boundary layer height where the airflow interacts with the terrain. We used the lifted condensation level (LCL) as indicator of the altitude at which the wind effect exerts the highest contribution to precipitation. The LCL has been calculated using the mean air temperature (tas) and mean relative humidity (RH) using:

$$LCL = 20 + (tas/5) * (100 - RH) \quad (11)$$

(Lawrence, 2005). The LCL has been interpolated to the CHELSA resolution using a B-spline interpolation. To create a boundary layer height corrected wind effect H_B The wind effect grid H containing was then proportionally distributed to all grid cells falling within a respective T31 grid cell using:

https://doi.org/10.5194/cp-2021-30
Preprint. Discussion started: 3 May 2021


Climate of the Past Discussions

$$H_B = \frac{H}{1-\left(\frac{|z-B|-z_{max}}{h}\right)} \quad (12)$$

With z_{max} being the being the maximum distance between the lifted condensation level LCL_z *at elevation* z and all grid cells at a 30 arc sec. resolution falling within a respective T31 grid cell, h being a constant of 9000 m, and z being the respective elevation from GMTED2010 (Danielson and Gesch, 2011) with:

$$LCL_z = LCL + z_{GCM} + f \quad (13)$$

B being the height of the monthly means of daily mean boundary layer from TraCE21k, z_{GCM} being the elevation of the TraCE21k grid cell, and f being a constant of 500 m which takes into account that the level of highest precipitation is not necessarily at the lower bound of the LCL, but slightly higher (Karger et al., 2017a).

The wind effect algorithm cannot distinguish extremely isolated valleys inside highly-elevated mountain areas (Frei and Schär, 1998). Such valleys are situated in areas where the wet air masses flow over an orographic barrier and are prevented from flowing into deep valleys. These effects are mainly confined to large mountain ranges, and are not as prominent in small- to intermediate-sized mountain ranges (Liu et al., 2012). Such dry valleys are situated in areas where the wet air masses flow over an orographic barrier and are prevented from flowing into deep valleys (Karger et al., 2020). To account for these effects, we used a variant of the windward leeward equations with a linear search distance of 300 km in steps of 5° from 0° to 355° circular for each grid cell. The calculated leeward index was then scaled towards higher elevations using:

$$E = \left(\frac{\sum_{i=1}^{n} \frac{1}{d_{WHi}} tan^{-1}\left(\frac{d_{LZi}}{d_{WHi}}\right)}{\sum_{i=1}^{n} \frac{1}{d_{LHi}}}\right)^{\frac{z}{h}} \quad (14)$$

c was set to 9000 m.. h has been set to 9000 m. $E * H_B$ will give the first approximation of precipitation intensity p_I.

To achieve the distribution of monthly precipitation pr_o given the approximated precipitation intensity p_{I_c} at each grid location (x_c, y_c), we used a linear relationship between p_m^{cor} and p_{I_c} using:

$$pr_o = \frac{p_{I_c}}{\frac{1}{n}\sum_{i=1}^{n} p_{I_{c_i}}} * p_m^{cor} \quad (15)$$

where n equals the number of 30 arc sec. grid cells that fall within a 0.25 grid cell.

https://doi.org/10.5194/cp-2021-30
Preprint. Discussion started: 3 May 2021

Climate of the Past Discussions

4 Output validation

Direct validation of the temperature (Fig 1) and precipitation (Fig. 2) output at high resolution for paleo time series generally relies on proxies, as direct observations of both variables are not available. Although global temperature time series exist, they only give global means, and do not allow validation of the performance of a 1km paleo climatic dataset. Therefore, to validate the CHELSA_TraCE21k dataset we complement a simple comparison of the simulated time series to proxy data and current observations, with approaches of validating derived parameters from the simulated temperature and precipitation that directly benefit from a very high horizontal resolution.

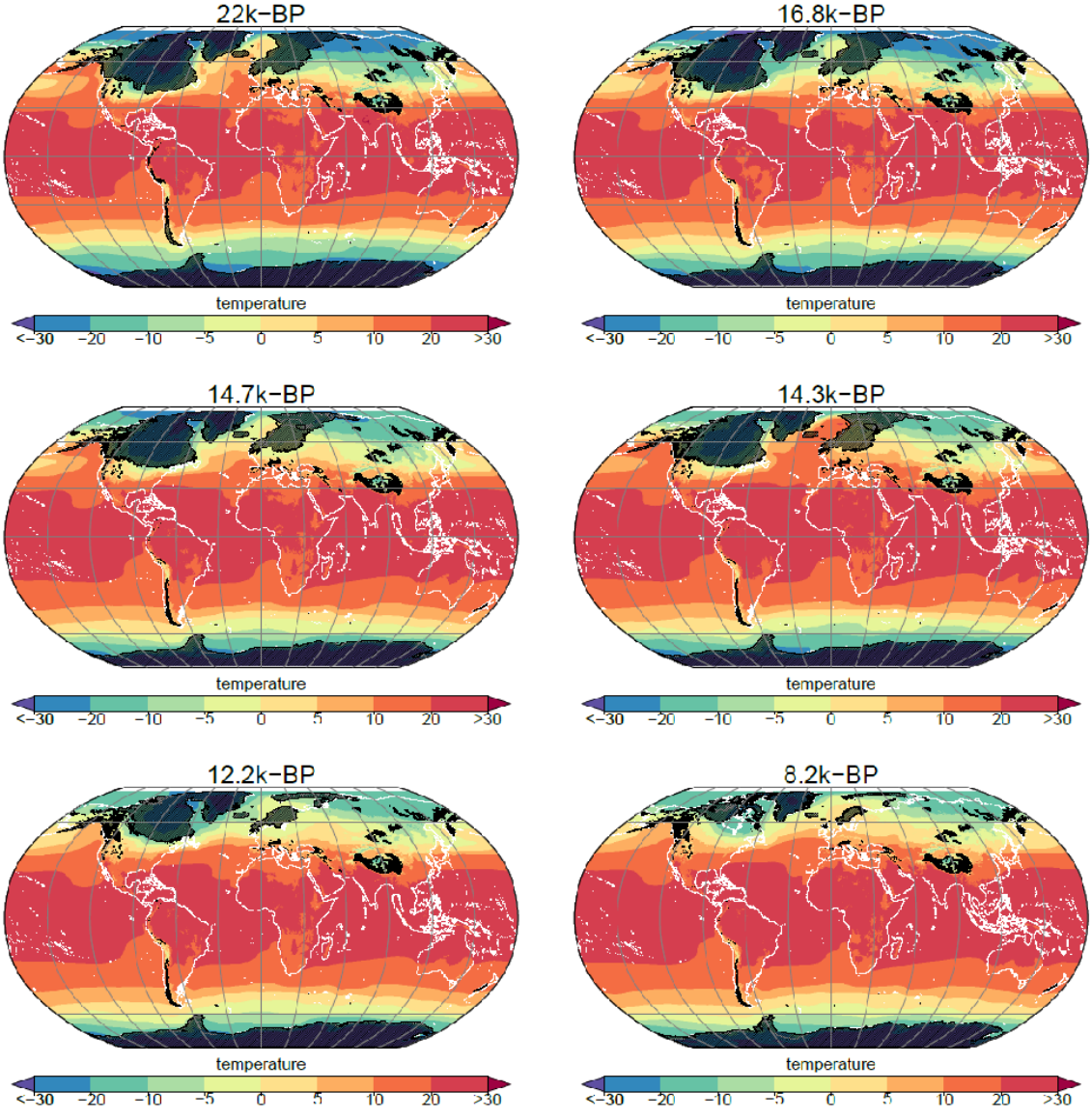

https://doi.org/10.5194/cp-2021-30
Preprint. Discussion started: 3 May 2021

Climate of the Past Discussions
Open Access
EGU

Figure 1: Mean annual near surface air temperature for time periods before present (BP) that showed exceptional climate dynamics in the northern Atlantic region, from the CHELSA_TraCE21k model. The interpolated extent of the glaciers at each time step is shown as shaded black polygons. The approximated coast lines are delineated in white. The last glacial maximum is shown for 22k-BP. The Heinrich I event, during which the northern Atlantic was actually colder compared to the LGM, is shown in 16.6k-BP. The extreme warming at the Bølling-Allerød is evident from the comparison of 14.7k-BP, shortly before the onset-, and 14.3k-BP, the maximum of the Bølling-Allerød warming. The middle of the Younger Dryas cold period is shown at 12.2k-BP. The 8.2 kiloyear event is shown at 8.2k-BP.

https://doi.org/10.5194/cp-2021-30
Preprint. Discussion started: 3 May 2021

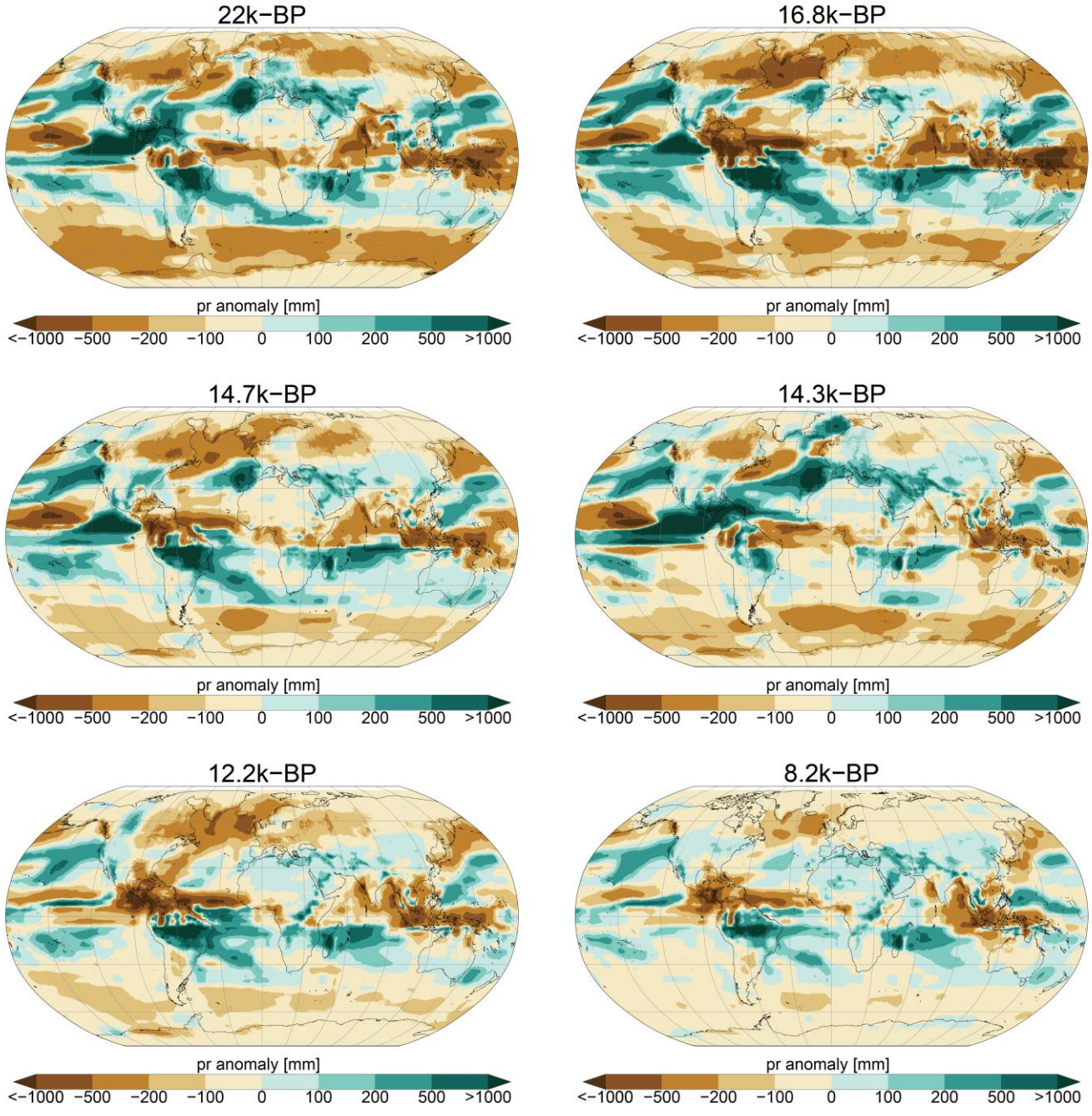

Figure 2: Anomalies in annual precipitation sums from the precipitation of the 1990 period for time periods before present (BP) that showed exceptional climate dynamics, from the CHELSA_TraCE21k model. The approximated coast lines are delineated in black. The last glacial maximum is shown for 22k-BP. The Heinrich I event, during which the northern Atlantic was actually colder and dryer compared to the LGM, is shown in 16.6k-BP. The extreme warming at the Bølling-Allerød with increased precipitation is evident from the comparison of 14.7k-BP, shortly before the onset-, and 14.3k-BP, the maximum of the Bølling-Allerød warming. The middle of the Younger Dryas, a cold period with lower precipitation in the northern Atlantic region, is shown at 12.2k-BP. The 8.2 kiloyear event is shown at 8.2k-BP. At this event, precipitation shows the lowest overall anomalies from current precipitation.

https://doi.org/10.5194/cp-2021-30
Preprint. Discussion started: 3 May 2021


Climate of the Past Discussions

265 **4.1 Validation using current (historical) observations**

We used data from the Global Historical Climate Network (GHCN) monthly database V.3 (Lawrimore et al., 2011) to validate the performance of the downscaling algorithm during the last time step of the CHELSA-TraCE21k for which station data is available. To do so we calculated monthly climatologies for each month for *tasmax*, *tasmin*, and *pr* from both TraCE21k and CHELSA-TraCE21k. We then compared the values measured at each station to that simulated in both, TraCE21k and
270 CHELSA-TraCE21k.

Although the downscaling algorithm might increase the performance of the temperature and precipitation estimates during the historical period, this does not imply that this improvement is equal during the entire transient time series. To further validate the data, we therefore compared it to more derived parameters for which time series data exists.

4.2 Comparison with temperature proxies from Ice core data

275 We compared the downscaled temperatures with the Greenland ice core reconstructions of Buizert et al. (Buizert et al., 2014, 2018) to check the performance of the downscaling at eight ice core locations on the Greenland Ice Shield (GIS). Although both temperature reconstructions and GCM generated temperatures have uncertainties connected to them (Erb et al., 2018), the ice core data are so far the best possible validation dataset that spans the entire deglaciation period from 21kBP to 1990 (Buizert et al., 2014, 2018). To assess the performance gain of the downscaling over the coarse resolution TraCE21k data, we
280 compare the ice core annual mean near surface temperature reconstructions with both the CHELSA-TraCE21k, and the original TraCE21k temperature data.

4.3 Validation of glacier extent between 18kPB and 1kBP

As the ice core temperature reconstructions have associated uncertainties, it is impossible to disentangle if potential differences between the ice core data and the model data are due to uncertainties in the reconstructions. To validate the downscaled
285 temperature data further, we used the interpolated extent of glaciers in CHELSA_TraCE21k, and compared it to glacial extent data from Dyke et al. 2003. The data consists of expert delineated glacier maps based on a chronological database of radiocarbon dates and contains >4000 dates located in North America (Dyke et al., 2003). To compare both datasets, we first calculated the glacial extent from CHELSA_TraCE21k by assigning each 1km gridcell in a Lambert Conformal Conic projection (+proj=lcc +lat_1=49 +lat_2=77 +lat_0=49 +lon_0=-95 +x_0=0 +y_0=0 +ellps=clrk66 +units=m +no_defs, extent=
290 x_{min}: -3698534, x_{max}: 3596392, y_{min}: -1259083, y_{max} : 4674296). to either to be covered by a glacier [1] or being free of glacier [0]. We assigned a 1 if the simulated glacier height was above the paleo terrain elevation, and a 0 if it was lower or equal to the paleo terrain elevation. The paleo terrain elevation was calculated using the current terrain elevation minus the sea level difference between current and that of the respective paleo timestep. As the current terrain elevation already includes extent glaciers, this elevation dependent procedure of assigning glacial extents would result in the current glaciers being assigned a
295 0. Therefore we assigned all grid cells covered by extent glaciers a 1.

https://doi.org/10.5194/cp-2021-30
Preprint. Discussion started: 3 May 2021

Climate of the Past Discussions

To compare the simulated glacial extent to the expert delineated extent, we rasterized the polygons provided by Dyke et al., 2003 for the years 18 kBP - 1 kBP to the 1km resolution, extent, and projection of the simulated glacial cover and assign a 1 where the polygon intersects with a 1km raster cell and a 0 otherwise.

We then calculated three different test values to identify if the simulations correctly predict the presence and absence of a glacier. As the dataset is highly unbalanced between absences of glaciers [0] and presences of glaciers [1] through time we use balanced accuracy which is defined as: (sensitivity+specificity)/2. Additionally we report Cohen's Kappa, and the True Skill Statistic (Allouche et al., 2006).

5 Validation results

5.1 Accuracy of temperature and precipitation estimated during the current (historical) period

The original TraCE21k data shows large deviations and root mean squared errors (RSME) from the observed data (Fig. 3). This is somewhat expected as a climate model running for such long time periods needs to have coarse resolution, as well as a large degree of generalism and realism which decreases the accuracy of a model when compared to observations. The temperature variables perform well in TraCE21k with r ~ 0.8 for all months, but have deviations and RSME similar to those of precipitation, that most likely can be attributed to the coarse resolution of the climate model. Trace21k also seems to overestimate temperature extremes both for *tasmax* and *tasmin* (Fig. 4).

The precipitation however, does not perform well in the model with r ~ 0.4 and large deviations from actual values (Fig. 3) and overall precipitation seems to be too low in the model (Fig. 4).

The downscaling algorithm improves the correlation between observed and modelled and decreases the standard deviation for all three parameters (Fig. 3). The downscaling for the temperature variables increases the correlation to r ~ 0.95 for all months and decreases the standard deviation substantially (Fig. 3). Similarly the performance of the precipitation estimation in CHELSA-TraCE21k increases, which is reflected in a r ~0.7 and a lower standard deviation and RSME (Fig. 3). The underestimation of precipitation in the TraCE21k is reduced, but the downscaling algorithm still has a considerable bias (Fig. 3) during the historical period.

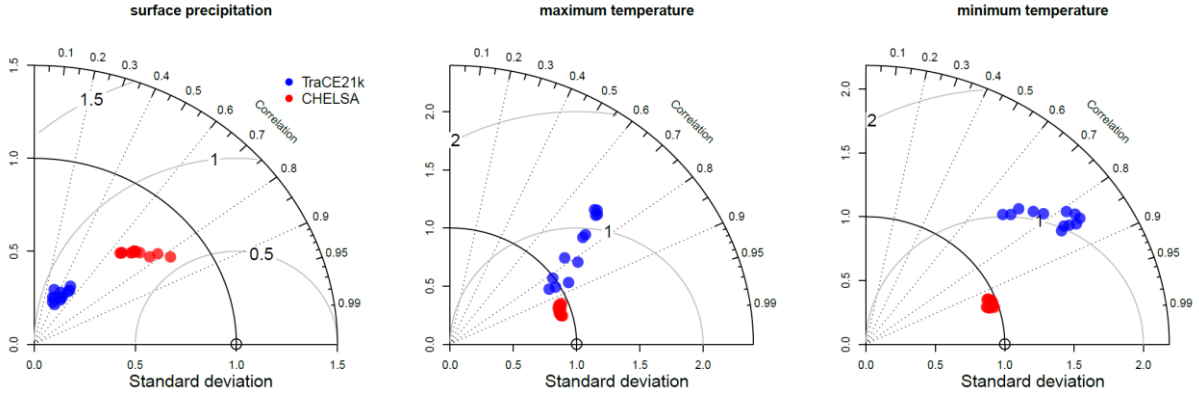

https://doi.org/10.5194/cp-2021-30
Preprint. Discussion started: 3 May 2021

Climate of the Past Discussions
Open Access
EGU

320 **Figure 3: Taylor plots comparing the relationship between f CCSM3-TraCE21k (blue) and CHELSA_TraCE21k (red).** Data is shown for the 20th century time period with observational data from the Global Historical Climate Network (GHCN) for the time period 1950-1990. Each dot represents a specific month.

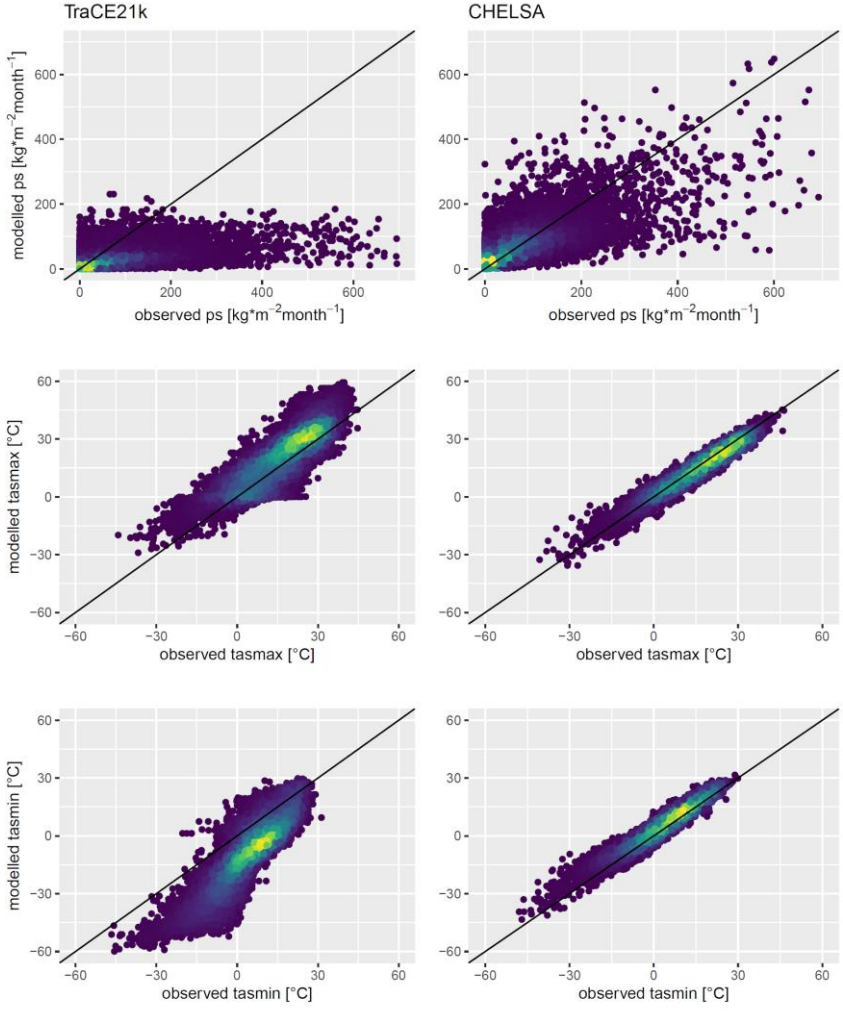

Figure 4: Scatter plots comparing precipitation, maximum-, and minimum temperature. Data are aggregated from TraCE21k and 325 CHELSA_TraCE21k for the 20th century time period with observational data from the Global Historical Climate Network (GHCN) for the time period 1900-1990.

5.2 Performance of the downscaling algorithms for temperatures compared to ice cores

Compared to the temperature reconstructions, the downscaled CHELSA_TraCE21k model had reduced bias at four of the ice 330 core sites located at the edges of the GIS (ReCAP, Agassiz, Hans Tausen Iskappe, Camp Century), but increased the bias, RMSE and MAE at the remaining four sites at the center of the GIS (NEEM, NGRIP, GISP2, Dye 3) (Fig. 5). Overall both

https://doi.org/10.5194/cp-2021-30
Preprint. Discussion started: 3 May 2021

Climate of the Past Discussions

CHELSA_TraCE as well as TraCE21k show a warm bias before the H1 event, and roughly after the 8.2k event at four of the sites (ReCAP, Agassiz, Hans Tausen Iskappe, Camp Century). At three sites (ReCAP, Agassiz, Hans Tausen Iskappe, Camp Century) a cold bias is present after the younger Dryas (Fig. 5). At the four other sites, the biases are idiosyncratic with CHELSA_TraCE usually showing a warm bias before the H1, and TraCE a cold bias before the H1 (Fig. 5). After the younger dryas, both models show a cold bias at these sites. At the Camp Century site, the Trace data are close to the δ^{15}N-based temperature reconstructions before the H1 event, and CHELSA_TraCE shows a warm bias, while after the younger dryas the situation is reversed (Fig. 5).

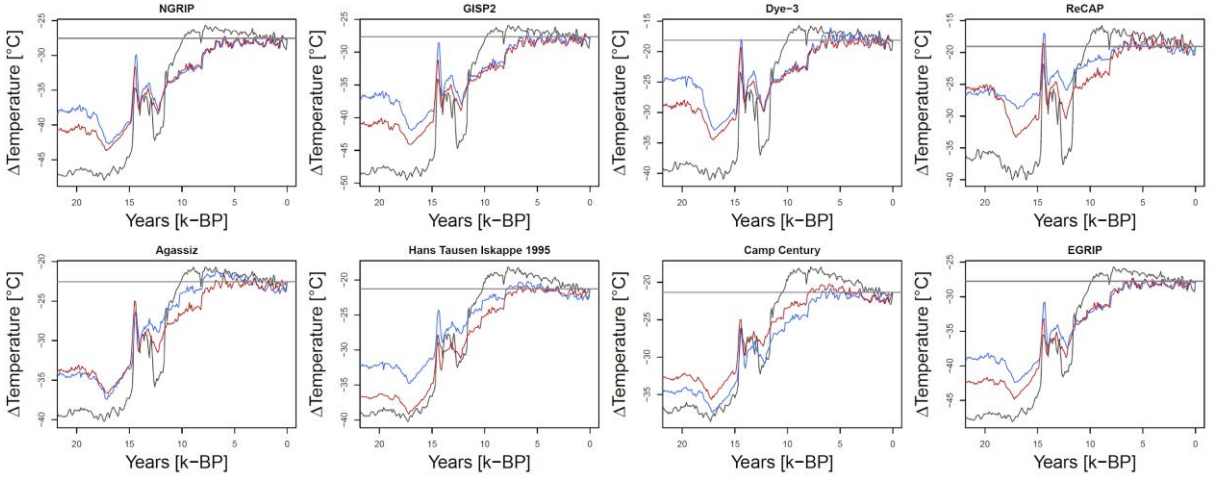

Figure 5: Comparison of temperature anomalies from current for the CHELSA-TraCE21k time series data (blue), the TraCE21k data (red), with the temperature reconstructions from ice cores (black) across Greenland. The grey line indicates the current observed temperature during the period 1981-2010 from CHELSA V2.1. Temperatures are plotted as anomalies from the current temperature recorded at the respective location of the ice cores.

5.3 Accuracy of the glacier extent between 18kPB and 1kBP

The test validations of the glacial extent show a good performance over most time steps (Fig. 6), but with a notable drop in accuracy at 8 kBP where all three validation metrics drop significantly. Aside from the drop at 8 kBP, the performance of the glacial extent simulations performed well. The marked drop in performance around 8 kBP might be due to the 8.2 kiloyear event, which marked a strong decrease in global temperatures, most likely due to meltwater fluxes from the collapsing Laurentide ice sheet. The strong coupling between temperature and glacial extent in CHELSA-TraCE21k generates an increase in glacial extent more than a sudden collapse during this time period, which seems to override the signal from the ICE6G forcing data in CHELSA-TraCE21k.

https://doi.org/10.5194/cp-2021-30
Preprint. Discussion started: 3 May 2021

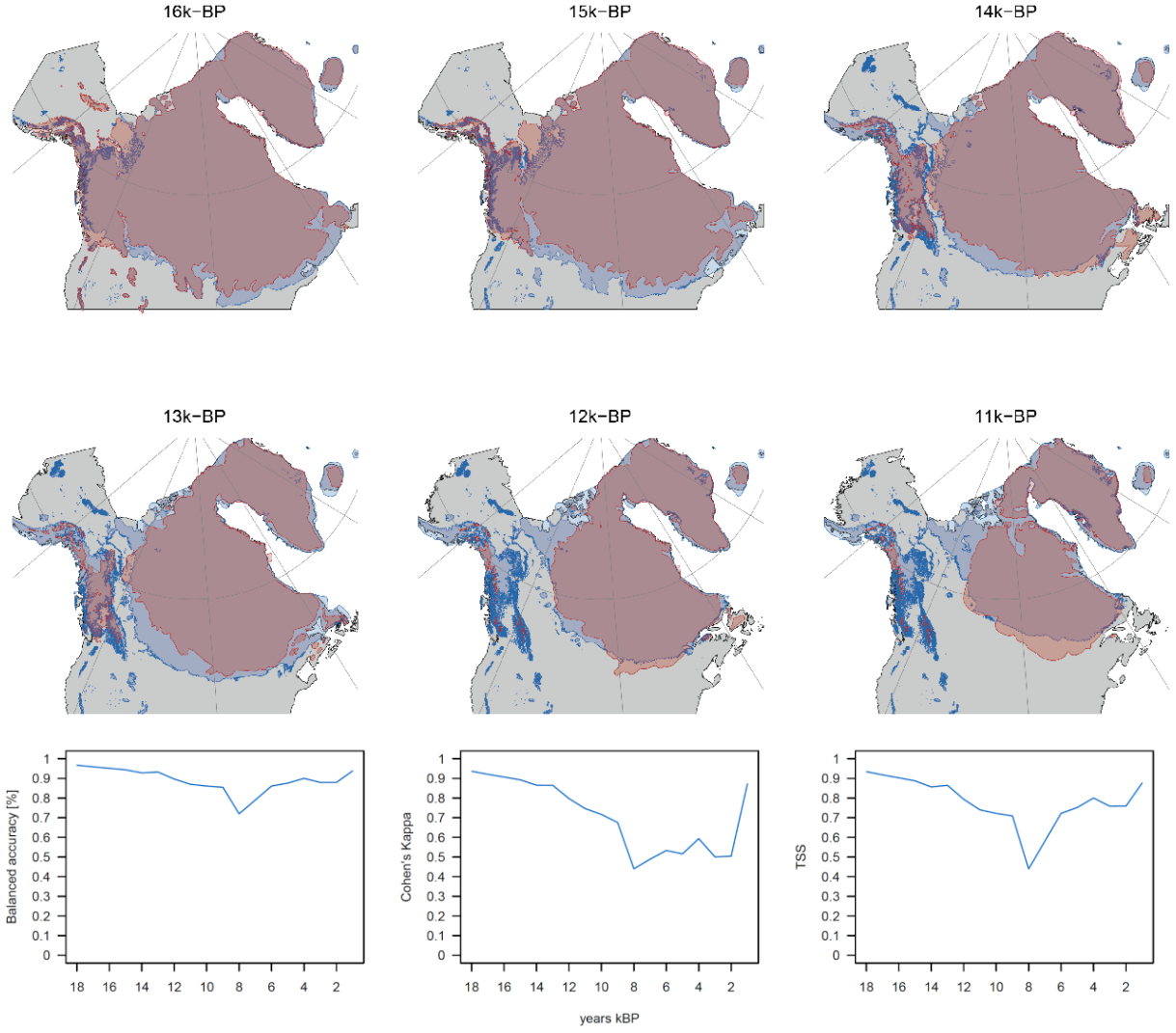

Figure 6: Comparisons of estimated glacial extents of the Laurentide ice shield from 16k-BP to 11k-BP. Blue delineates the interpolated ice shield extent from CHELSA-TraCE21k, and red shows the estimated extent from (Dyke et al., 2003). While the retreat of the main Laurentide ice shield is similar in both estimations, the Cordilleran Ice shield covering the Rocky Mountains, retreats faster in the estimations by (Dyke et al., 2003), compared to CHELSA-TraCE21. b.) Performance comparison using three different metrics (Balanced accuracy, Cohen's Kappa, and True Skill Statistic) from a comparison of CHELSA-TraCE21k and Dyke et al. 2003.

6 Potential applications: Dynamic simulation of effective refugia

Transient long term climatic data have a wide range of possible applications. Here we want to highlight a possible application in paleo-ecology by using the climate data to detect LGM refugia of plant species. Climatic changes during the last glacial

https://doi.org/10.5194/cp-2021-30
Preprint. Discussion started: 3 May 2021


Climate of the Past Discussions

cycle since the LGM, have had a significant influence on the distribution of ecosystems (Williams and Jackson, 2007), species (Hampe and Jump, 2011; Hewitt, 1999), and as a result on intraspecific genetic structures and speciation (Alsos et al., 2012; Pellissier et al., 2015; Yannic et al., 2014, 2020).

Tracing the distribution of species through time is, however, challenging as the the spatio-temporal distributions of species strongly depend on environmental suitability (Guisan and Zimmermann, 2000), spatial accessibility of a given location (Normand et al., 2011; Svenning and Skov, 2004), and species dispersal abilities (Engler and Guisan, 2009). A dynamic simulation of species distributions can integrate all these aspects and therefore provides a valuable testbed for paleoclimatic data (Nobis and Normand, 2014). However, the spatio-temporal resolution of climate data needed for such simulations have been limited to comparable coarse grain climatic data (Gherghel and Martin, 2020), which usually creates a mismatch between the climate derived from the model and the climate actually experienced by an organism (Seo et al., 2009).

Here, we use the downscaled transient temperature and precipitation data since 17kyBP (the coldest recorded temperatures in the TracCE21k model for Europe) to reconstruct refugia of the deciduous tree Grey Alder (Alnus incana) in Europe before post glacial climate warming. Similar to Nobis & Normand (2014), we first calibrated a generalized linear model (GLM) (Nelder and Wedderburn, 1972) using current presences and absences of Grey Alder within polygons of the Atlas Florae Europaeae (AFE) (Kurtto et al., 2018) as the response variable and current annual mean temperature and precipitation from CHELSA-TraCE21k as predictors calculated as zonal mean values of 5 x 5 km rasterized AFE polygons. Despite the simplicity of the model it showed a fair to good model fit with a 10-fold cross-validated AUC value of 0.89.

Then, the GLM model was used to predict the suitability of Grey Alder from 17kBP till today in 500-year steps with 5 km resolution and Lambert azimuthal equal-area projection. Glaciated areas were defined as unsuitable and were taken from the CHELSA-TraCE21k glacial reconstructions. We used the resulting time series of climatic suitability as input to the KISSMig model (Nobis & Normand 2014), which iteratively uses a simple 3 x 3 cell algorithm to calculate the spatial spread from a given origin from17kyBP to present. Presences and absences were weighted equally for the initial GLM calibration and KISSMig used squared suitability values to fulfill basic empirical expectations (see http://purl.oclc.org/wsl/kissmig).

We tested for each AFE polygon of the current Grey Alder distribution all 25 x 25 km areas across Europe as potential refugia. All 5 x5 km grid cells of those areas suitable at 17kyBP were kept as refugia, if the respective AFE polygon was accessible and the spread pattern generated the lowest number of false positives when compared to the current AFE distribution. Because the migration ability of Grey Alder was unknown a priori, KISSMig simulations used one to 10 iterations for each 500-year step, corresponding to a maximum migration rate of 10 to 100 m/yr. For each iteration number the combined spread pattern from all detected effective refugia was compared with the current distribution based on F1-scores. The optimized iteration number was identified by optimizing F1, which showed for Grey Alder a maximum migration rate of 50 m/yr. For a comparison with genetic clusters (Dering et al., 2016), the locations of that study were linked to the detected effective refugia with the shortest euclidean distance for simplicity.

Current genetic clustering of populations indicates that the modelling of A. incana distributions at 17kyBP successfully detected glacial refugia in the Southern Alps, southern Norway, northern Norway, the Balkans, and eastern Romania (Fig. 7).

https://doi.org/10.5194/cp-2021-30
Preprint. Discussion started: 3 May 2021

The situation in eastern Europe is more complex, with most refugia located in Russia. However, since we only used the current distribution of A. incana in western Europe the results might be biased towards the east.

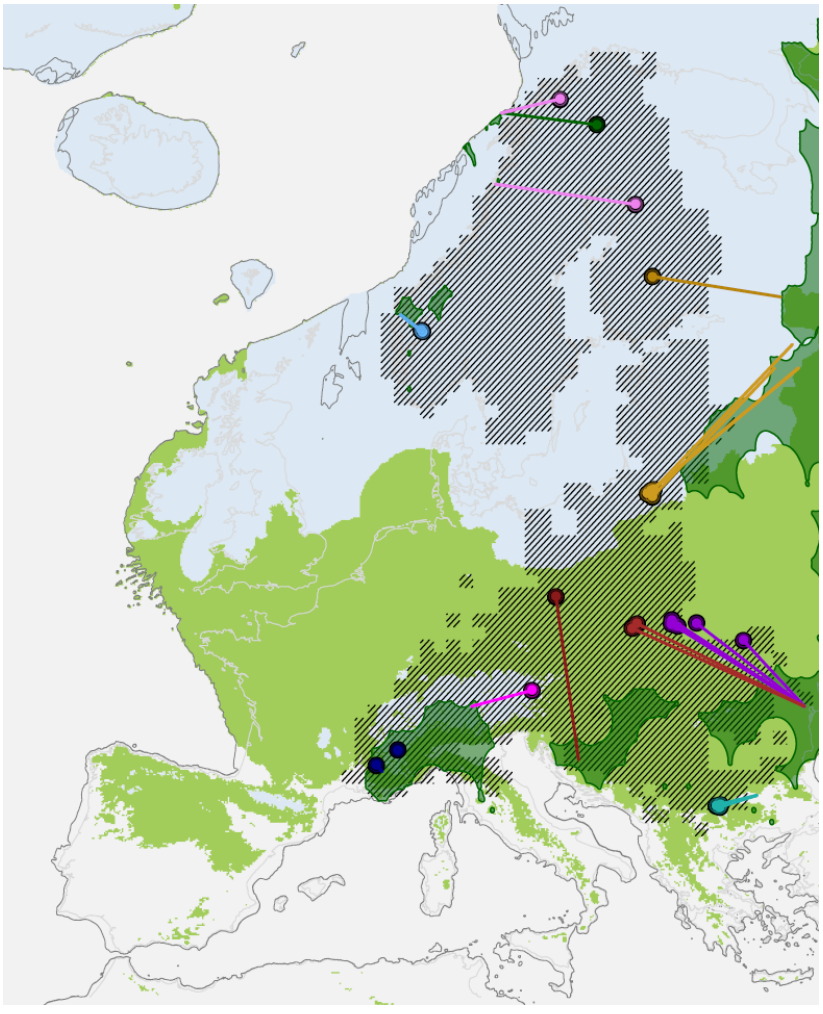

Figure 7: Distribution of *Alnus incana* in Europe (based on the Atlas Flora Europaea (Kurtto et al., 2018)) at current time (line shaded/hatched), and reconstructed effective refugia at 17kBP (dark green alpha hull polygons) using dynamic species distribution modelling based on KISSMig and CHELSA_TraCE21k. The entire suitable habitat for A. incana at 17kyBP is indicated as light green. Although almost the entire Europe was suitable for *A. incana* at 17kyBP, it might have not been at all locations due to dispersal constraints. Colored circles indicate the population genetic structure of *A. incana*, taken from Dering et al. 2016, where each color represents a genetic cluster. Lines indicate the most likely effective refugia a genetic cluster can be associated to, given dispersal and climatic constraints. Current genetic clustering of populations indicates that the modelling of *A. incana* distributions at 17kyBP successfully detected glacial effective refugia in the Southern Alps (dark blue), southern Norway (light blue), northern Norway (pink), the Balkans (dark red), and eastern Romania (turquoise), and the black sea (dark red and violet). As we only use the current distribution of *A. incana* within the AFE extent the results might be biased outside of it.

https://doi.org/10.5194/cp-2021-30
Preprint. Discussion started: 3 May 2021

7 Conclusions

Although both, the original TraCE21k, as well as the downscaled CHELSA-Trace21k data track the relative temperature change well compared to ice cores, both models have relatively high temperature biases in absolute temperatures. Both the original data and the downscaled data have a warm bias before the younger Dryas, and a cold bias after it relative to the ice core proxy data. There are several reasons for this: coupled atmosphere ocean general circulation models (GCMs) such as CCSM3 cannot provide regional-scale or unbiased information on a variety of climatic processes (Meehl et al., 2007). Temperatures from ice cores themselves are only based on proxy data, and the overall performance of such proxy data in estimating absolute temperatures is connected to biases in itself (Erb et al., 2018). The downscaling of the CHELSA-Trace21k data involves a trend-preserving (Hempel et al., 2013) change factor step to explicitly preserve the trends in TraCE21k. If however, these trends are already underestimated by the TraCE21k data, they will also be present in the downscaled data.

The estimation of glacial extents works comparably well when compared to expert delineations of the glacial extent of the Laurentide ice shield. There is, however, a clear drop in performance at the 8.4kY event when atmospheric methane concentration decreased leading to a cooling and drying of the northern hemisphere (Kobashi et al., 2007). The strong coupling of the ice interpolations with only temperature might cause the decrease in performance as the downscaling algorithm ignores changes in precipitation which is only present in the driving ICE6G data. As the downscaling assumes an increase in glacial boundaries with cooling, this effect might not be realistic under an overall drying climate, and the fast shifts in temperatures over only 150 years (Kobashi et al., 2007) might also not be well represented in a model with 100 year resolution. Another problem in the estimation of the glacial extent might be the result of the applied B-spline interpolation. The resulting ice cover from this interpolation can, in some areas, only be a few meters thick, not representing real glaciers, but rather spatial autocorrelation artefact of the interpolation approach used.

The CHELSA-Trace21k data seems to be able to recreate the distribution of temperature and precipitation in a meaningful manner, so that the use of the data in subsequent analysis produces meaningful results. The reconstruction of the refugia for *Alnus incana* shows that the combination of high resolution climate data, together with a dynamic distribution model was able to accurately detect refugia, even those of a few kilometers in extent (Parducci et al., 2012) that cannot be detected using coarse climate data.

Code availability

Downscaling codes are based on (Karger et al., 2017a), and all modules used are open source and integrated into SAGA-GIS, available here: https://sourceforge.net/projects/saga-gis/. The code unique to this study is written in R and creates the paleo-orography and glacier interpolations, and is also available on zenodo (DOI:10.5281/zenodo.4545753).

https://doi.org/10.5194/cp-2021-30
Preprint. Discussion started: 3 May 2021

Data availability

All post-processed data (Karger et al., 2021) and additional input files other than those provided by TraCE21k can be accessed at the envidat.ch (DOI:10.16904/envidat.211.). The data is published under a Creative Commons Attribution 2.0 Generic (CC BY 2.0) license.

Author contribution

D.N.K., M.N., and N.Z. developed the idea. D.N.K. developed the model and implemented the code. D.N.K. M.N. and S.N. validated the data. N.Z., S.N., and C.H.G. funded the project. D.N.K. wrote the first version of the manuscript and all authors contributed to subsequent revisions.

Competing interest

The authors declare that they have no conflict of interest.

Acknowledgements

D.N.K. & N.E.Z. acknowledge funding from: The WSL internal grants exCHELSA and ClimEx, the Joint Biodiversa COFUND Call on "Biodiversity and Climate Change" (project 'FeedBaCks') with the national funder Swiss National Foundation (20BD21_193907), as well as the Swiss Data Science Projects: SPEEDMIND, and COMECO. D.N.K. & C.H.G. acknowledges funding to the ERA-Net BiodivERsA - Belmont Forum, with the national funder Swiss National Foundation (20BD21_184131), part of the 2018 Joint call BiodivERsA-Belmont Forum call (project 'FutureWeb'), the WSL internal grant ClimEx. S.N. acknowledge funding from Aarhus University Research Foundation.

References

Adams, J. M. and Faure, H.: Preliminary Vegetation Maps of the World since the Last Glacial Maximum: An Aid to Archaeological Understanding, J. Archaeol. Sci., 24(7), 623–647, https://doi.org/10.1006/jasc.1996.0146, 1997.

Allouche, O., Tsoar, A. and Kadmon, R.: Assessing the accuracy of species distribution models: prevalence, kappa and the true skill statistic (TSS), J. Appl. Ecol., 43(6), 1223–1232, https://doi.org/10.1111/j.1365-2664.2006.01214.x, 2006.

Alsos, I. G., Ehrich, D., Thuiller, W., Eidesen, P. B., Tribsch, A., Schönswetter, P., Lagaye, C., Taberlet, P. and Brochmann, C.: Genetic consequences of climate change for northern plants, Proc. R. Soc. B Biol. Sci., 279(1735), 2042–2051, https://doi.org/10.1098/rspb.2011.2363, 2012.

Argus, D. F., Peltier, W. R., Drummond, R. and Moore, A. W.: The Antarctica component of postglacial rebound model ICE-6G_C (VM5a) based on GPS positioning, exposure age dating of ice thicknesses, and relative sea level histories, Geophys. J. Int., 198, 537–563, https://doi.org/10.1093/gji/ggu140, 2014.

https://doi.org/10.5194/cp-2021-30
Preprint. Discussion started: 3 May 2021

Basist, A., Bell, G. D. and Meentemeyer, V.: Statistical Relationships between Topography and Precipitation Patterns, J. Clim., 7(9), 1305–1315, https://doi.org/10.1175/1520-0442(1994)007<1305:SRBTAP>2.0.CO;2, 1994.

Berrisford, P., Dee, D., Fielding, K., Fuentes, M., Kallberg, P., Kobayashi, S. and Uppala, S.: The ERA-interim archive, ERA Rep. Ser., (1), 1–16, 2009.

Biasutti, M., Yuter, S. E., Burleyson, C. D. and Sobel, A. H.: Very high resolution rainfall patterns measured by TRMM precipitation radar: seasonal and diurnal cycles, Clim. Dyn., 39(1–2), 239–258, https://doi.org/10.1007/s00382-011-1146-6, 2011.

Binney, H., Edwards, M., Macias-Fauria, M., Lozhkin, A., Anderson, P., Kaplan, J. O., Andreev, A., Bezrukova, E., Blyakharchuk, T., Jankovska, V., Khazina, I., Krivonogov, S., Kremenetski, K., Nield, J., Novenko, E., Ryabogina, N., Solovieva, N., Willis, K. and Zernitskaya, V.: Vegetation of Eurasia from the last glacial maximum to present: Key biogeographic patterns, Quat. Sci. Rev., 157, 80–97, https://doi.org/10.1016/j.quascirev.2016.11.022, 2017.

Böhner, J.: General climatic controls and topoclimatic variations in Central and High Asia, Boreas, 35(2), 279–295, https://doi.org/10.1111/j.1502-3885.2006.tb01158.x, 2006.

Böhner, J. and Antonic, O.: Böhner, J., & Antonic, O. (2009). Land-Surface Parameters Specific to Topo-Climatology. In T. Hengl, & H. I. Reuter (Eds.), GEOMORPHOMETRY: CONCEPTS, SOFTWARE, APPLICATIONS (pp. 195-226). Elsevier Science., in in T. Hengl, & H. I. Reuter (eds.) Geomorphometry: Concepts, Software, Applications, pp. 195–226, Elsevier Science, , 2009.

Brown, J. L., Hill, D. J., Dolan, A. M., Carnaval, A. C. and Haywood, A. M.: PaleoClim, high spatial resolution paleoclimate surfaces for global land areas, Sci. Data, 5(1), 1–9, https://doi.org/10.1038/sdata.2018.254, 2018.

Buizert, C., Gkinis, V., Severinghaus, J. P., He, F., Lecavalier, B. S., Kindler, P., Leuenberger, M., Carlson, A. E., Vinther, B., Masson-Delmotte, V., White, J. W. C., Liu, Z., Otto-Bliesner, B. and Brook, E. J.: Greenland temperature response to climate forcing during the last deglaciation, Science, 345(6201), 1177–1180, https://doi.org/10.1126/science.1254961, 2014.

Buizert, C., Keisling, B. A., Box, J. E., He, F., Carlson, A. E., Sinclair, G. and DeConto, R. M.: Greenland-Wide Seasonal Temperatures During the Last Deglaciation, Geophys. Res. Lett., 45(4), 1905–1914, https://doi.org/10.1002/2017GL075601, 2018.

Carlson, A. E., Ullman, D. J., Anslow, F. S., He, F., Clark, P. U., Liu, Z. and Otto-Bliesner, B. L.: Modeling the surface mass-balance response of the Laurentide Ice Sheet to Bølling warming and its contribution to Meltwater Pulse 1A, Earth Planet. Sci. Lett., 315–316, 24–29, https://doi.org/10.1016/j.epsl.2011.07.008, 2012.

Collins, W. D., Bitz, C. M., Blackmon, M. L., Bonan, G. B., Bretherton, C. S., Carton, J. A., Chang, P., Doney, S. C., Hack, J. J., Henderson, T. B., Kiehl, J. T., Large, W. G., McKenna, D. S., Santer, B. D. and Smith, R. D.: The Community Climate System Model Version 3 (CCSM3), J. Clim., 19(11), 2122–2143, https://doi.org/10.1175/JCLI3761.1, 2006.

Daly, C., Taylor, G. H. and Gibson, W. P.: The PRISM approach to mapping precipitation and temperature, Proc 10th AMS Conf Appl. Climatol., 20–23, 1997.

Danielson, J. J. and Gesch, D. B.: Global multi-resolution terrain elevation data 2010 (GMTED2010), US Geological Survey., 2011.

Dyke, A. S., Moore, A. and Robertson, L.: Deglaciation of North America, 2003.

Ehlers, J., Gibbard, P. L. and Hughes, P. D.: Quaternary Glaciations - Extent and Chronology, Volume 15 - 1st Edition., 2011.

Engler, R. and Guisan, A.: MigClim: Predicting plant distribution and dispersal in a changing climate, Divers. Distrib., 15(4), 590–601, https://doi.org/10.1111/j.1472-4642.2009.00566.x, 2009.

Erb, M. P., Jackson, C. S., Broccoli, A. J., Lea, D. W., Valdes, P. J., Crucifix, M. and DiNezio, P. N.: Model evidence for a seasonal bias in Antarctic ice cores, Nat. Commun., 9(1), 1361, https://doi.org/10.1038/s41467-018-03800-0, 2018.

Frei, C. and Schär, C.: A precipitation climatology of the Alps from high-resolution rain-gauge observations, Int. J. Climatol., 18(8), 873–900, https://doi.org/10.1002/(SICI)1097-0088(19980630)18:8<873::AID-JOC255>3.0.CO;2-9, 1998.

Frieler, K., Lange, S., Piontek, F., Reyer, C. P. O., Schewe, J., Warszawski, L., Zhao, F., Chini, L., Denvil, S., Emanuel, K., Geiger, T., Halladay, K., Hurtt, G., Mengel, M., Murakami, D., Ostberg, S., Popp, A., Riva, R., Stevanovic, M., Suzuki, T., Volkholz, J., Burke, E., Ciais, P., Ebi, K., Eddy, T. D., Elliott, J., Galbraith, E., Gosling, S. N., Hattermann, F., Hickler, T., Hinkel, J., Hof, C., Huber, V., Jägermeyr, J., Krysanova, V., Marcé, R., Müller Schmied, H., Mouratiadou, I., Pierson, D., Tittensor, D. P., Vautard, R., Vliet, M. van, Biber, M. F., Betts, R. A., Bodirsky, B. L., Deryng, D., Frolking, S., Jones, C. D., Lotze, H. K., Lotze-Campen, H., Sahajpal, R., Thonicke, K., Tian, H. and Yamagata, Y.: Assessing the impacts of 1.5 °C global warming – simulation protocol of the Inter-Sectoral Impact Model Intercomparison Project (ISIMIP2b), Geosci. Model Dev., 10(12), 4321–4345, https://doi.org/10.5194/gmd-10-4321-2017, 2017.

Fuhrer, O., Chadha, T., Hoefler, T., Kwasniewski, G., Lapillonne, X., Leutwyler, D., Lüthi, D., Osuna, C., Schär, C., Schulthess, T. C. and Vogt, H.: Near-global climate simulation at 1km resolution: establishing a performance baseline on 4888 GPUs with COSMO 5.0, Geosci. Model Dev., 11(4), 1665–1681, https://doi.org/10.5194/gmd-11-1665-2018, 2018.

Funk, C., Verdin, A., Michaelsen, J., Peterson, P., Pedreros, D. and Husak, G.: A global satellite-assisted precipitation climatology, Earth Syst Sci Data, 7(2), 275–287, https://doi.org/10.5194/essd-7-275-2015, 2015.

Gao, X., Xu, Y., Zhao, Z., Pal, J. S. and Giorgi, F.: On the role of resolution and topography in the simulation of East Asia precipitation, Theor. Appl. Climatol., 86(1–4), 173–185, https://doi.org/10.1007/s00704-005-0214-4, 2006.

Gherghel, I. and Martin, R. A.: Postglacial recolonization of North America by spadefoot toads: integrating niche and corridor modeling to study species' range dynamics over geologic time, Ecography, 43(10), 1499–1509, https://doi.org/10.1111/ecog.04942, 2020.

Guisan, A. and Thuiller, W.: Predicting species distribution: offering more than simple habitat models, Ecol. Lett., 8(9), 993–1009, 2005.

Guisan, A. and Zimmermann, N. E.: Predictive habitat distribution models in ecology, Ecol. Model., 135, 147–186, 2000.

Hampe, A. and Jump, A. S.: Climate Relicts: Past, Present, Future, Annu. Rev. Ecol. Evol. Syst., 42(1), 313–333, https://doi.org/10.1146/annurev-ecolsys-102710-145015, 2011.

Harris, I., Osborn, T. J., Jones, P. and Lister, D.: Version 4 of the CRU TS monthly high-resolution gridded multivariate climate dataset, Sci. Data, 7(1), 1–18, https://doi.org/10.1038/s41597-020-0453-3, 2020.

He, F.: Simulating Transient Climate Evolution of the Last Deglaciation with CCSM3, PhD - Thesis, University of Wisconsin Madison, Madison, WC, USA, 2011.

Hempel, S., Frieler, K., Warszawski, L., Schewe, J. and Piontek, F.: A trend-preserving bias correction–the ISI-MIP approach, Earth Syst. Dyn., 4(2), 219–236, 2013.

Hewitt, G. M.: Post-glacial re-colonization of European biota, Biol. J. Linn. Soc., 68(1–2), 87–112, https://doi.org/10.1111/j.1095-8312.1999.tb01160.x, 1999.

Hijmans, R. J., Cameron, S. E., Parra, J. L., Jones, P. G. and Jarvis, A.: Very high resolution interpolated climate surfaces for global land areas, Int. J. Climatol., 25(15), 1965–1978, https://doi.org/10.1002/joc.1276, 2005.

Huffman, G. J., Bolvin, D. T., Nelkin, E. J., Wolff, D. B., Adler, R. F., Gu, G., Hong, Y., Bowman, K. P. and Stocker, E. F.: The TRMM Multisatellite Precipitation Analysis (TMPA): Quasi-Global, Multiyear, Combined-Sensor Precipitation Estimates at Fine Scales, J. Hydrometeorol., 8(1), 38–55, https://doi.org/10.1175/JHM560.1, 2007.

Hunter, R. D. and Meentemeyer, R. K.: Climatologically Aided Mapping of Daily Precipitation and Temperature, J. Appl. Meteorol., 44(10), 1501–1510, https://doi.org/10.1175/JAM2295.1, 2005.

Hutchinson, G. E.: POPULATION STUDIES - ANIMAL ECOLOGY AND DEMOGRAPHY - CONCLUDING REMARKS, Cold Spring Harb. Symp. Quant. Biol., 22, 415–427, 1957.

Karger, D. N., Conrad, O., Böhner, J., Kawohl, T., Kreft, H., Soria-Auza, R. W., Zimmermann, N. E., Linder, H. P. and Kessler, M.: Climatologies at high resolution for the earth's land surface areas, Sci. Data, 4, 170122, 2017a.

Karger, D. N., Conrad, O., Böhner, J., Kawohl, T., Kreft, H., Soria-Auza, R. W., Zimmermann, N. E., Linder, H. P. and Kessler, M.: Climatologies at high resolution for the earth's land surface areas, Dryad Digital Repository., 2017b.

Karger, D. N., Schmatz, D. R., Dettling, G. and Zimmermann, N. E.: High resolution monthly precipitation and temperature timeseries for the period 2006-2100, Sci. Data, 2020.

Karger, D. N., Nobis, M., Normand, S., Graham, C. H. and Zimmermann, N. E.: CHELSA-TraCE21k: Downscaled transient temperature and precipitation data since the last glacial maximum - EnviDat, envidat, https://doi.org/10.16904/envidat.211., 2021.

Kobashi, T., Severinghaus, J. P., Brook, E. J., Barnola, J.-M. and Grachev, A. M.: Precise timing and characterization of abrupt climate change 8200 years ago from air trapped in polar ice, Quat. Sci. Rev., 26(9), 1212–1222, https://doi.org/10.1016/j.quascirev.2007.01.009, 2007.

Körner, C.: The use of 'altitude' in ecological research, Trends Ecol. Evol., 22(11), 569–574, https://doi.org/10.1016/j.tree.2007.09.006, 2007.

Kurtto, A., Sennikov, A. B. and Lampinen, R.: Atlas Florae Europaeae - Distribution of vascular plants in Europe, Comm. Mapp. Flora Eur. Soc. Biol. Fenn. Vanamo Hels. 132 Pp, 23(1), 106–106, 2018.

Lawrence, M. G.: The Relationship between Relative Humidity and the Dewpoint Temperature in Moist Air: A Simple Conversion and Applications, Bull. Am. Meteorol. Soc., 86(2), 225–234, https://doi.org/10.1175/BAMS-86-2-225, 2005.

Lawrimore, J. H., Menne, M. J., Gleason, B. E., Williams, C. N., Wuertz, D. B., Vose, R. S. and Rennie, J.: An overview of the Global Historical Climatology Network monthly mean temperature data set, version 3, J. Geophys. Res.-Atmospheres, 116(D19121), D19121, https://doi.org/10.1029/2011jd016187, 2011.

https://doi.org/10.5194/cp-2021-30
Preprint. Discussion started: 3 May 2021

Liu, M., Bárdossy, A. and Zehe, E.: Interaction of valleys and circulation patterns (CPs) on small-scale spatial precipitation distribution in the complex terrain of southern Germany., Hydrol. Earth Syst. Sci. Discuss., 9(12), 2012.

Liu, Z., Otto-Bliesner, B. L., He, F., Brady, E. C., Tomas, R., Clark, P. U., Carlson, A. E., Lynch-Stieglitz, J., Curry, W., Brook, E., Erickson, D., Jacob, R., Kutzbach, J. and Cheng, J.: Transient Simulation of Last Deglaciation with a New Mechanism for Bølling-Allerød Warming, Science, 325(5938), 310–314, https://doi.org/10.1126/science.1171041, 2009.

Maraun, D.: Bias correction, quantile mapping, and downscaling: Revisiting the inflation issue, J. Clim., 26(6), 2137–2143, 2013.

Maraun, D.: Bias Correcting Climate Change Simulations - a Critical Review, Curr. Clim. Change Rep., 2(4), 211–220, https://doi.org/10.1007/s40641-016-0050-x, 2016.

Maraun, D., Wetterhall, F., Ireson, A. M., Chandler, R. E., Kendon, E. J., Widmann, M., Brienen, S., Rust, H. W., Sauter, T., Themeßl, M., Venema, V. K. C., Chun, K. P., Goodess, C. M., Jones, R. G., Onof, C., Vrac, M. and Thiele-Eich, I.: Precipitation downscaling under climate change: Recent developments to bridge the gap between dynamical models and the end user, Rev. Geophys., 48(3), RG3003, https://doi.org/10.1029/2009RG000314, 2010.

Marcott, S. A., Clark, P. U., Padman, L., Klinkhammer, G. P., Springer, S. R., Liu, Z., Otto-Bliesner, B. L., Carlson, A. E., Ungerer, A., Padman, J., He, F., Cheng, J. and Schmittner, A.: Ice-shelf collapse from subsurface warming as a trigger for Heinrich events, Proc. Natl. Acad. Sci., 108(33), 13415–13419, https://doi.org/10.1073/pnas.1104772108, 2011.

McMaster, G. S. and Wilhelm, W.: Growing degree-days: one equation, two interpretations, 1997.

Meehl, G. A., Stocker, T. F., Collins, W. D., Friedlingstein, P., Gaye, A. T., Gregory, J. M., Kitoh, A., Knutti, R., Murphy, J. M., Noda, A., Raper, S. C. B., Watterson, I. G., Weaver, A. J. and Zhao, Z.-C.: Global climate projections, in Climate Change 2007: The Physical Science Basis. Contribution of Working Group I to the Fourth Assessment Report of the Intergovernmental Panel on Climate Change, Cambridge University Press, Cambridge, UK, , 2007.

Meyer-Christoffer, A., Becker, A., Finger, P., Rudolf, B., Schneider, U. and Ziese, M.: GPCC Climatology Version 2015 at 0.25°: Monthly Land-Surface Precipitation Climatology for Every Month and the Total Year from Rain-Gauges built on GTS-based and Historic Data., Glob. Precip. Climatol. Cent. GPCC, https://doi.org/10.5676/DWD_GPCC/CLIM_M_V2015_025, 2015.

Miller, K. G., Kominz, M. A., Browning, J. V., Wright, J. D., Mountain, G. S., Katz, M. E., Sugarman, P. J., Cramer, B. S., Christie-Blick, N. and Pekar, S. F.: The Phanerozoic Record of Global Sea-Level Change, Science, 310(5752), 1293–1298, https://doi.org/10.1126/science.1116412, 2005.

Nelder, J. A. and Wedderburn, R. W. M.: Generalized Linear Models, J. R. Stat. Soc. Ser. Gen., 135(3), 370–384, https://doi.org/10.2307/2344614, 1972.

Neumann, P., Düben, P., Adamidis, P., Bauer, P., Brück, M., Kornblueh, L., Klocke, D., Stevens, B., Wedi, N. and Biercamp, J.: Assessing the scales in numerical weather and climate predictions: will exascale be the rescue?, Philos. Trans. R. Soc. Math. Phys. Eng. Sci., 377(2142), 20180148, https://doi.org/10.1098/rsta.2018.0148, 2019.

Nobis, M. P. and Normand, S.: KISSMig – a simple model for R to account for limited migration in analyses of species distributions, Ecography, 37(12), 1282–1287, https://doi.org/10.1111/ecog.00930, 2014.

https://doi.org/10.5194/cp-2021-30
Preprint. Discussion started: 3 May 2021

Normand, S., Ricklefs, R. E., Skov, F., Bladt, J., Tackenberg, O. and Svenning, J.-C.: Postglacial migration supplements climate in determining plant species ranges in Europe, Proc. R. Soc. Lond. B Biol. Sci., rspb20102769, https://doi.org/10.1098/rspb.2010.2769, 2011.

Oke, T. R.: Boundary layer climates, Routledge., 2002.

Otto-Bliesner, B. L., Brady, E. C., Clauzet, G., Tomas, R., Levis, S. and Kothavala, Z.: Last Glacial Maximum and Holocene Climate in CCSM3, J. Clim., 19(11), 2526–2544, https://doi.org/10.1175/JCLI3748.1, 2006.

Pellissier, L., Eidesen, P. B., Ehrich, D., Descombes, P., Schönswetter, P., Tribsch, A., Westergaard, K. B., Alvarez, N., Guisan, A., Zimmermann, N. E., Normand, S., Vittoz, P., Luoto, M., Damgaard, C., Brochmann, C., Wisz, M. S. and Alsos, I. G.: Past climate-driven range shifts and population genetic diversity in arctic plants, J. Biogeogr., n/a-n/a, https://doi.org/10.1111/jbi.12657, 2015.

Peltier, W. R.: Global glacial isostasy and the surface of the ice-age earth: The ICE-5G (CM2) Model and GRACE, Annu. Rev. Earth Planet. Sci., 32(1), 111–149, https://doi.org/10.1146/annurev.earth.32.082503.144359, 2004.

Peltier, W. R., Argus, D. F. and Drummond, R.: Space geodesy constrains ice age terminal deglaciation: The global ICE-6G_C (VM5a) model, J. Geophys. Res. Solid Earth, 120(1), 450–487, https://doi.org/10.1002/2014JB011176, 2015.

Prentice, I. C., Bartlein, P. J. and Webb, T.: Vegetation and Climate Change in Eastern North America Since the Last Glacial Maximum, Ecology, 72(6), 2038–2056, https://doi.org/10.2307/1941558, 1991.

Raup, B., Racoviteanu, A., Khalsa, S. J. S., Helm, C., Armstrong, R. and Arnaud, Y.: The GLIMS geospatial glacier database: A new tool for studying glacier change, Glob. Planet. Change, 56(1), 101–110, https://doi.org/10.1016/j.gloplacha.2006.07.018, 2007.

Rotunno, R. and Houze, R. A.: Lessons on orographic precipitation from the Mesoscale Alpine Programme, Q. J. R. Meteorol. Soc., 133(625), 811–830, https://doi.org/10.1002/qj.67, 2007.

Schär, C., Fuhrer, O., Arteaga, A., Ban, N., Charpilloz, C., Di Girolamo, S., Hentgen, L., Hoefler, T., Lapillonne, X., Leutwyler, D., Osterried, K., Panosetti, D., Rüdisühli, S., Schlemmer, L., Schulthess, T., Sprenger, M., Ubbiali, S. and Wernli, H.: Kilometer-scale climate models: Prospects and challenges, Bull. Am. Meteorol. Soc., 101(5), https://doi.org/10.1175/BAMS-D-18-0167.1, 2019.

Schmidli, J., Frei, C. and Vidale, P. L.: Downscaling from GCM precipitation: a benchmark for dynamical and statistical downscaling methods, Int. J. Climatol., 26(5), 679–689, https://doi.org/10.1002/joc.1287, 2006.

Schulthess, T. C., Bauer, P., Wedi, N., Fuhrer, O., Hoefler, T. and Schär, C.: Reflecting on the goal and baseline for exascale computing: a roadmap based on weather and climate simulations, Comput. Sci. Eng., 21(1), 30–41, 2018.

Scotese, C. R.: Atlas of earth history, PALEOMAP project., 2001.

Seo, C., Thorne, J. H., Hannah, L. and Thuiller, W.: Scale effects in species distribution models: implications for conservation planning under climate change, Biol. Lett., 5(1), 39–43, https://doi.org/10.1098/rsbl.2008.0476, 2009.

Sepulchre, P., Caubel, A., Ladant, J.-B., Bopp, L., Boucher, O., Braconnot, P., Brockmann, P., Cozic, A., Donnadieu, Y., Dufresne, J.-L., Estella-Perez, V., Ethé, C., Fluteau, F., Foujols, M.-A., Gastineau, G., Ghattas, J., Hauglustaine, D., Hourdin, F., Kageyama, M., Khodri, M., Marti, O., Meurdesoif, Y., Mignot, J., Sarr, A.-C., Servonnat, J., Swingedouw, D.,

https://doi.org/10.5194/cp-2021-30
Preprint. Discussion started: 3 May 2021

Szopa, S. and Tardif, D.: IPSL-CM5A2 – an Earth system model designed for multi-millennial climate simulations, Geosci. Model Dev., 13(7), 3011–3053, https://doi.org/10.5194/gmd-13-3011-2020, 2020.

Sevruk, B.: Regional Dependency of Precipitation-Altitude Relationship in the Swiss Alps, in Climatic Change at High Elevation Sites, edited by H. F. Diaz, M. Beniston, and R. S. Bradley, pp. 123–137, Springer Netherlands, https://doi.org/10.1007/978-94-015-8905-5_7, , 1997.

Skamarock, C., Klemp, B., Dudhia, J., Gill, O., Liu, Z., Berner, J., Wang, W., Powers, G., Duda, G., Barker, D. and Huang, X.: A Description of the Advanced Research WRF Model Version 4, OpenSky, https://doi.org/10.5065/1dfh-6p97, 2019.

Soria-Auza, R. W., Kessler, M., Bach, K., Barajas-Barbosa, P. M., Lehnert, M., Herzog, S. K. and Bohner, J.: Impact of the quality of climate models for modelling species occurrences in countries with poor climatic documentation: a case study from Bolivia, Ecol. Model., 221(8), 1221–1229, 2010.

Spreen, W. C.: A determination of the effect of topography upon precipitation, Eos Trans. Am. Geophys. Union, 28(2), 285–290, https://doi.org/10.1029/TR028i002p00285, 1947.

Stull, R. B.: An introduction to boundary layer meteorology, Springer Science & Business Media., 2012.

Svenning, J.-C. and Skov, F.: Limited filling of the potential range in European tree species, Ecol. Lett., 7(7), 565–573, https://doi.org/10.1111/j.1461-0248.2004.00614.x, 2004.

Velichko, A. A., Andreev, A. A. and Klimanov, V. A.: Climate and vegetation dynamics in the tundra and forest zone during the late glacial and holocene, Quat. Int., 41–42, 71–96, https://doi.org/10.1016/S1040-6182(96)00039-0, 1997.

Weischet, W. and Endlicher, W.: Einführung in die Allgemeine Klimatologie, Schweizerbart Science Publishers, Stuttgart, Germany. https://www.schweizerbart.de/publications/detail/isbn/9783443071424/Einfhrung-in-die-Allgemeine-Klimatologie, last access: 20 June 2020, 2008.

Wilby, R. L., Wigley, T. M. L., Conway, D., Jones, P. D., Hewitson, B. C., Main, J. and Wilks, D. S.: Statistical downscaling of general circulation model output: A comparison of methods, Water Resour. Res., 34(11), 2995–3008, https://doi.org/10.1029/98WR02577, 1998.

Williams, J. W. and Jackson, S. T.: Novel climates, no-analog communities, and ecological surprises, Front. Ecol. Environ., 5(9), 475–482, 2007.

Williams, J. W., Shuman, B. N., III, T. W., Bartlein, P. J. and Leduc, P. L.: Late-Quaternary Vegetation Dynamics in North America: Scaling from Taxa to Biomes, Ecol. Monogr., 74(2), 309–334, 2004.

Willmott, C. J. and Robeson, S. M.: Climatologically aided interpolation (CAI) of terrestrial air temperature, Int. J. Climatol., 15(2), 221–229, https://doi.org/10.1002/joc.3370150207, 1995.

Wood, A. W., Leung, L. R., Sridhar, V. and Lettenmaier, D. P.: Hydrologic Implications of Dynamical and Statistical Approaches to Downscaling Climate Model Outputs, Clim. Change, 62(1–3), 189–216, https://doi.org/10.1023/B:CLIM.0000013685.99609.9e, 2004.

Woodward, F. I., Fogg, G. E., Heber, U., Laws, R. M. and Franks, F.: The impact of low temperatures in controlling the geographical distribution of plants, Philos. Trans. R. Soc. Lond. B Biol. Sci., 326(1237), 585–593, https://doi.org/10.1098/rstb.1990.0033, 1990.

https://doi.org/10.5194/cp-2021-30
Preprint. Discussion started: 3 May 2021

Yannic, G., Pellissier, L., Ortego, J., Lecomte, N., Couturier, S., Cuyler, C., Dussault, C., Hundertmark, K. J., Irvine, R. J., Jenkins, D. A., Kolpashikov, L., Mager, K., Musiani, M., Parker, K. L., Røed, K. H., Sipko, T., Þórisson, S. G., Weckworth, B. V., Guisan, A., Bernatchez, L. and Côté, S. D.: Genetic diversity in caribou linked to past and future climate change, Nat. Clim. Change, 4(2), 132–137, https://doi.org/10.1038/nclimate2074, 2014.

Yannic, G., Hagen, O., Leugger, F., Karger, D. N. and Pellissier, L.: Harnessing paleo-environmental modeling and genetic data to predict intraspecific genetic structure, Evol. Appl., 13(6), 1526–1542, https://doi.org/10.1111/eva.12986, 2020.

Yu, Z., Loisel, J., Brosseau, D. P., Beilman, D. W. and Hunt, S. J.: Global peatland dynamics since the Last Glacial Maximum, Geophys. Res. Lett., 37(13), https://doi.org/10.1029/2010GL043584, 2010.